JOURNAL GEOLOGICAL SOCIETY OF INDIA
Vol.75, January 2010, pp.278-288

Natural Electromagnetic Radiation (EMR) and its Application in Structural Geology and Neotectonics

REINHARD O. GREILING[1] and HENNES OBERMEYER[2]
[1]Institut für Angewandte Geowissenschaften, Universität Karlsruhe (TH), Hertzstrasse 16, 76187 Karlsruhe, Germany
[2]Gesellschaft für Erkundung and Ortung, Yorckstrasse 36, 76183 Karlsruhe, Germany
[1]**Email:**er8@agk.uka.de

Abstract: Natural electromagnetic radiation (EMR) impulses are emitted from rocks under stress. Electromagnetic emission may start during crystal deformation prior to and during the nucleation phase of nanocracks. The emission direction is either parallel with or normal to the crack surfaces. The EMR magnetic component is measured by the sensor or aerial of an instrument, the Cerescope, at frequencies from 5 to 50 kHz. Measurements at the surface show directions of recent stresses remarkably well. A calibration of EMR intensity in terms of stress magnitude is possible in tunnels, where the overburden pressure can be calculated. Two examples from the Upper Rhine Graben and NW India show EMR line measurements. In both cases, stress concentrations at fault or bedding surfaces can be detected. These surfaces can be regarded as tectonically active. Two further examples of EMR determinations in tunnels give more detailed information on the regional stress field. The example from the Swiss Jura fold-and-thrust belt shows directional results, with different directions beneath and above the regional detachment horizon at the base of the belt. The example from central Scandinavia shows a late Caledonian shear zone as a boundary between two recent stress domains, and gives absolute values of stress.

Keywords: Natural electromagnetic radiation (EMR), Neotectonics, Nanofractures, Active faults, Recent stress.

INTRODUCTION

During the last few decades, field observations and laboratory experiments have shown the existence of natural electromagnetic radiation (EMR), which is emitted from rocks under stress. The nature of such EMR pulses is well known from laboratory experiments (e.g. Rabinovitch at al. 1996, 2002; Bahat et al. 2005, and references therein): the closer a material is brought to its limit of fracture strength and to frictional sliding the more nanofractures are formed and the more electromagnetic pulses are emitted. Electromagnetic emission may also start during crystal deformation prior to and during the nucleation phase of nanocracks. Due to the cracking of bonds between ions, a polarization occurs at the cracks. Any relative movement of the polarized crack walls gives rise to the emission of EMR. Since this relative movement of the crack walls is controlled by the crack orientation, the emission direction of EMR is also related to the crack orientation. Therefore, the EMR emission direction is either parallel with or normal to the crack surfaces (e.g. Lichtenberger, 2006a, c; Reuther and Moser, 2007). Figure 1 gives a schematic view of a rock volume with a crack or fracture and EMR originating from it. In this example, the EMR propagation direction is normal to the crack. The EMR signal is composed of an electric and a magnetic component, which are both normal to each other and to the EMR propagation direction. The magnetic component is measured by the sensor or aerial of an instrument, which is called the Cerescope (see below). Although the physical explanation is not always straightforward, it is now well established that EMR directions can be related to the directions of nanofractures and their causative stresses (e.g. Bahat et al. 2005; Lichtenberger, 2006c). As a consequence, EMR measurements may be evaluated in order to determine the directions of recently active stresses and the regional stress field. Single EMR impulses may last a few milliseconds (ms). Groups of such electromagnetic impulses at a 100ms time scale are called bursts. Single impulses can be related to low stress. Bursts indicate relatively higher stress (Frid, 1997, 2001; Bahat et al. 2005; Lichtenberger, 2006c). Accordingly, measurements of EMR intensity can also be used to compare relative intensities and thus values of stress. In that way, zones or areas of relatively high recent stresses may be located. Therefore, EMR determinations

are being used successfully for problems of slope or tunnel stability and other engineering geological topics (e.g. Frid, 1997, 2001; Liu and He, 2001; Obermeyer et al. 2001; Lauterbach, 2002; Wang et al. 2005). However, EMR information is also useful for scientific problems, for example stress concentrations at particular fracture surfaces, and neotectonics in general (e.g. Reuther et al. 2002; Bahat et al. 2005; Lichtenberger, 2005; 2006a, b, c; Reuther and Moser, 2007; Mallik et al. 2008).

The present paper intends to give a short introduction into natural EMR and its measurement. In addition, four examples of the application of EMR studies to neotectonic problems are presented here, in order to show the possibilities of EMR application in structural geology in different tectonic environments.

MEASUREMENT OF NATURAL PULSED ELECTROMAGNETIC RADIATION (EMR) WITH THE CERESCOPE

The Cerescope is an instrument for the detection and registration of transient pulses of electromagnetic radiation (EMR). It comprises two major parts, a sensor or aerial, and a computing unit, which also contains the power supply and related technical components, as they are shown in Figure 2. The sensor of the Cerescope is a particular ferrite aerial, which is most sensitive for the magnetic, h-component of the electromagnetic field (Fig. 1) at a frequency of 12.8 kHz. The Cerescope is built to pick up impulses in a frequency range from 5 kHz to 50 kHz. Such a frequency range corresponds to a "penetration depth" of tens to hundreds of m (see Lichtenberger, 2006c; Reuther and Moser, 2007; for details). Accordingly, the registered signals represent EMR from a corresponding rock volume surrounding the Cerescope measuring point. Penetration depth is dependent on the EMR frequency, with a relatively lower depth at higher frequencies. Therefore, EMR information for a practical problem may be obtained from a limited rock volume close to the measuring point, when using only 50 kHz, or for a larger volume when using lower frequencies.

All incoming signals are registered and stored during a period of 100 ms. Signal processing and computing takes place in a subsequent period which lasts approximately 900 ms. In order to keep it flexible and to perform maximum selectivity, the Cerescope is adjusted to a pulse averaging mode that discriminates various background noises effectively. Typical anthropogenic radio waves can be filtered automatically. Alternatively, the user has the possibility to perform a graphically indicated frequency analysis (Fig. 2c) in order to identify non-geogenic radiation, or interfering radio waves. Such radio waves are distinct by a clearly defined peak at their particular frequency (Figs. 2c; also see Fig. 8a). In contrast, natural EMR covers a wide range of frequencies (e.g. Bahat et al. 2005).

The results are displayed either graphically or numerically with a dynamic range of true 16 bit. Qualities of the impulses can be represented in different ways: impulse numbers (counts), number of bursts, typical frequency, typical amplitude, energy of pulses. It has to be noted that these are not absolute values but depend on the amplification and discrimination settings of the Cerescope as described above. Hence, EMR intensities are mostly given as relative values or arbitrary units. According to the Cerescope measurement routine, these units refer to a time period of 100ms. Over a corresponding interface the stored data can be transferred to any computer with a RS-232 interface. Necessary software to transfer data to Microsoft Excel is provided with the Cerescope. The Cerescope can be carried and operated by a single person even

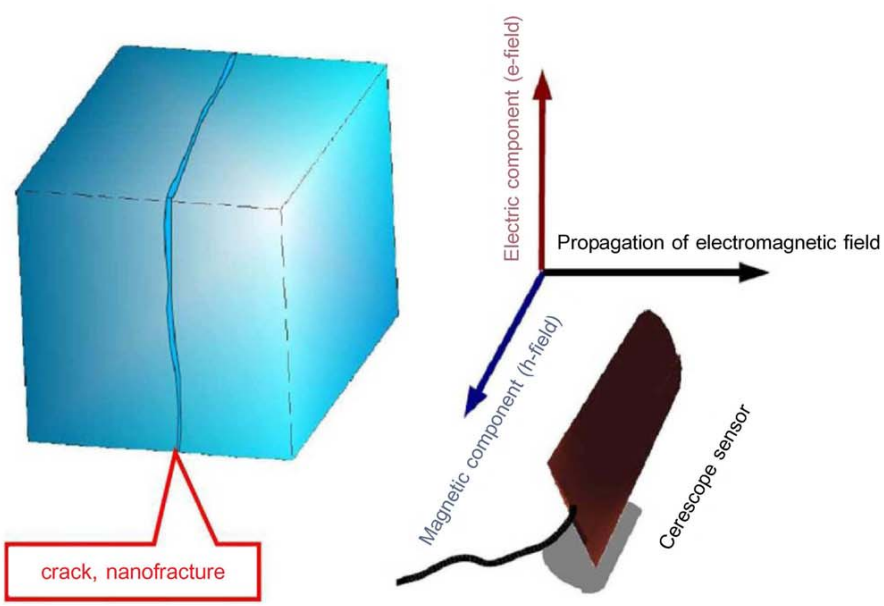

Fig.1. Sketch of a rock volume with a crack, related EMR, which is composed of electric and magnetic componenents, and an aerial for EMR measurement (Cerescope sensor).

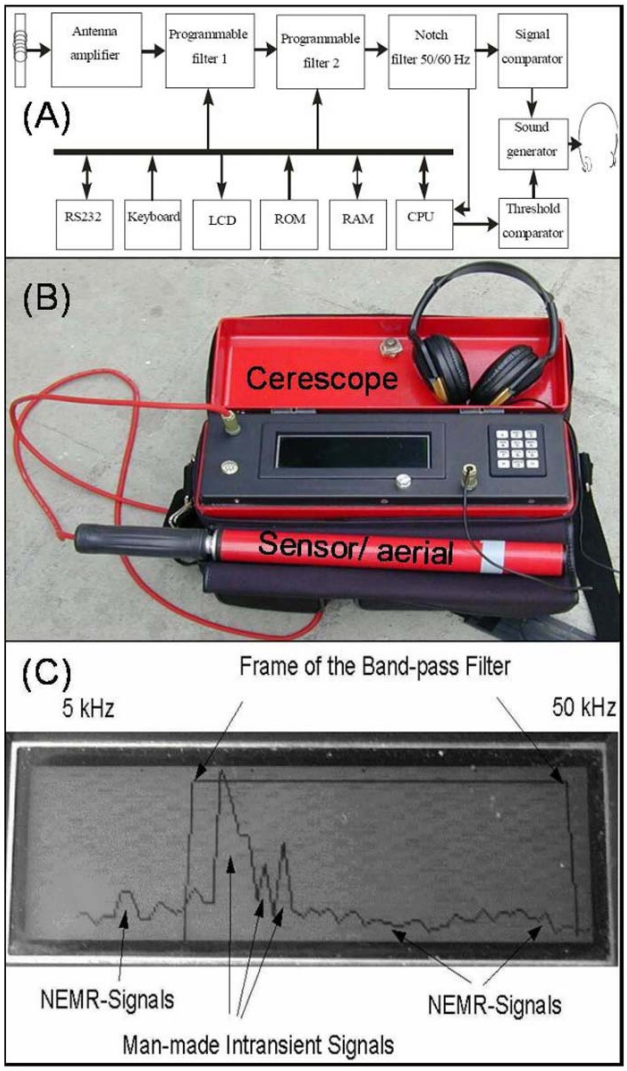

Fig.2. Details of the Cerescope instrument for EMR detection and processing. **(a)** Layout of Cerescope for natural EMR determination and evaluation, with aerial (signal input) at top left and data output either acoustically (right) or as data files (bottom left). CPU: Central Processing Unit, RAM: Random Access Memory, ROM: Read-Only Memory, LCD: Liquid Crystal Display, RS232: Serial Port. **(b)** Photograph of Cerescope instrument and sensor/aerial. The latter is 30cm long, excluding the handle. **(c)** Display of Cerescope (detail of b, LCD of a), showing the full range of frequencies between 5 kHz and 50 kHz. The operator may change the size and position of the band-pass filter in order to exclude unwanted, anthropogenic signals.

in a rough terrain or underground. The aerial can also be adjusted for drill hole measurements.

MEASUREMENT METHODS

If the Cerescope sensor or aerial is aligned parallel with nanofractures emitting EMR, it will register their corresponding impulses at a maximum intensity. However, if the aerial is pointed downwards, towards the earth's surface, it will pick up a bulk signal. This bulk signal corresponds to a particular "bulk stress magnitude". The Cerescope allows to measure consecutively at a time interval of 1 second (s). In that way, measuring points can be combined into line measurements, similar to other geophysical measurement methods (e.g. Parasnis,1996; Milsom, 2003). As a result, the measured line shows relative EMR intensities or stress values. Peak values indicate stress concentrations and may be interpreted as loci of active or potentially active fracture surfaces. A symmetric peak can be related to a vertical surface, oblique peaks may be related to inclined fracture surfaces (see below and Figs. 4b, 5c).

Orienting the Cerescope aerial in a horizontal position allows to determine directions and relative magnitude of horizontal stresses. Such horizontal measurements are best performed along a (horizontal) full circle at 5º or 10º intervals, depending on the desired accuracy. Results can be compiled into a direction rose (Fig. 3a). In general, one to four major peaks can be observed. As outlined in detail by Lichtenberger (2006c) and Reuther and Moser (2007), a single peak is interpreted as due to extensional fractures. As a consequence, the direction of the fractures is parallel with that of the maximum horizontal stress. Two or four peaks can generally be related to shear fractures. In that case, the maximum horizontal stress direction is in the direction of the bisector of two conjugate peaks.

Similar to the horizontal directional measurements, EMR may also be determined in a vertical circle in the underground, for example in a tunnel. There, the vertical circle is oriented normal to the tunnel axis (Fig. 3b). In general, results show four conjugate peaks at c. 45º, 135°, 225°, and 315°, respectively, counting from the top at 0°. These peaks can be related to a set of conjugate shear fractures, striking along the tunnel axis and dipping 45° towards either side (Lichtenberger, 2006a, b, c). As a consequence of this shear fracture and stress distribution in a tunnel, line measurements along a tunnel axis should be performed with the aerial inclined at c. 45º in order to pick up a good EMR signal (see Fig. 3c and Lichtenberger, 2006a, b, c).

Measurements at the surface show directions of recent stresses remarkably well (e.g. Obermeyer et al. 2001; Reuther et al. 2002; Lichtenberger, 2006a, b, c; Reuther and Moser, 2007) but not their absolute magnitude. However, a calibration of EMR intensity in terms of stress magnitude is possible if the value of the vertical component can be

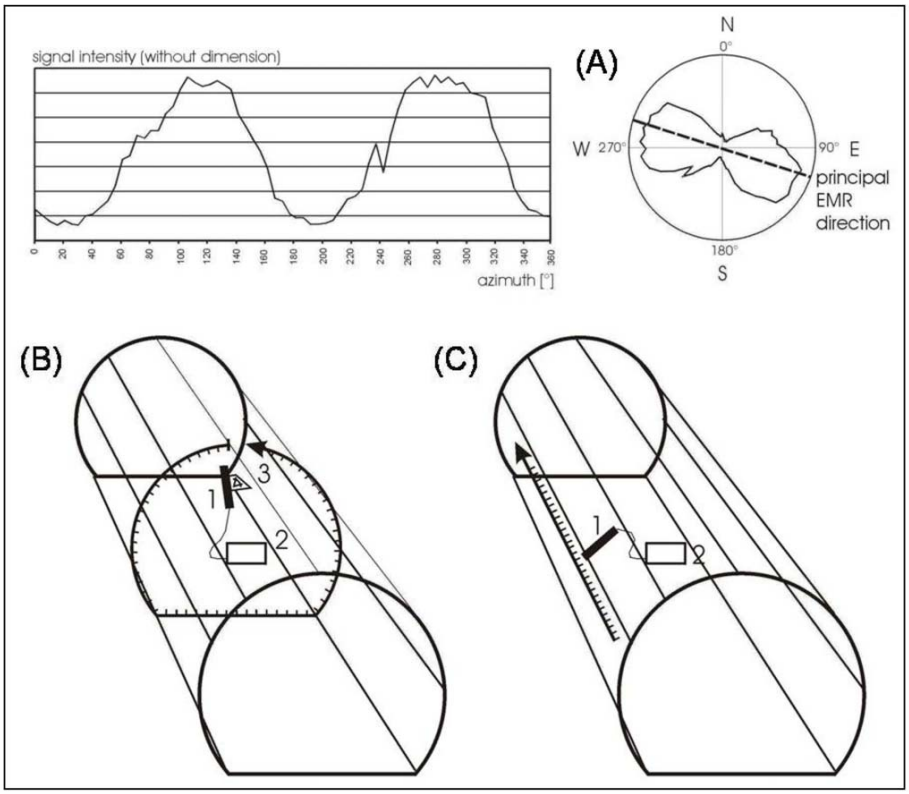

Fig.3. EMR measurement methods. **(a)** Horizontal, directional measurement, with display from 0º to 360º and corresponding direction rose. **(b)** Vertical directional measurement in a tunnel, data output as in (a); 1: Cerescope sensor/aerial, 2: Cerescope instrument, 3: clinometer. **(c)** Linear measurement in a tunnel with the aerial inclined at c. 45º; numbers as in (b).

determined. Lichtenberger (2005; 2006b) showed that the shear stress in a tunnel is at a minimum, where the overburden pressure is equal to the maximum horizontal stress. He calculated the overburden pressure from the height of the rock column above the tunnel at the shear stress minimum. This value corresponds not only to the vertical stress component but is also equal to the horizontal stress component normal to the tunnel.

HORIZONTAL, DIRECTIONAL EMR MEASUREMENTS AND STRUCTURAL APPLICATIONS

In order to show the application of EMR line measurements, two examples are outlined here. One of these is from the Upper Rhine Graben (Germany), a major continental rift with both extensional and strike-slip components. The second example is from the Kachchh area in NW India, where recent compressional and strike-slip deformation is well documented.

Marginal Fault of the Upper Rhine Graben Rift

The Upper Rhine Graben (URG) is a major continental rift in central Europe, which extends for almost 300 km in length and c. 40 km in width. It is bound in the east by the Black Forest and Odenwald hills, in the west by the Vosges and Pfälzer Wald hills, which form the morphological expression of the rift shoulders. The present rift basin floor is covered by Quaternary sediments, which, in places, are fringed by Paleogene and Neogene rocks. Information on the structural evolution and stress distribution of the URG is available from earlier studies (e.g. Schumacher, 2001; Dèzes et al. 2004; Rotstein et al. 2005; Cardozo and Behrmann, 2006). Accordingly, the early evolution started with extension in E-W direction during Paleogene times. Subsequent sinistral transform movement terminated before Plio-Pleistocene times. The irregular geometry of the active faults in the URG caused along-strike changes in deformational character, with local transpression in the south, mostly strike-slip movement in the centre, and transtension in the north. Following Schumacher (2001), the northern part of the URG is a pull-apart basin with N-S extension. Other studies, however, documented an E-W asymmetry, with subsidence concentrated at the eastern margin of the northern URG (e.g. Haimberger et al. 2005; Peters and van Balen, 2006; Peters, 2007). According to Dèzes et al. (2004) and Reinecker et al. (2004), regional horizontal stresses are compressive, with a maximum in NW-SE direction (Fig. 4a). In addition, recent stresses are also influenced by local fault geometries and easy-slip horizons (see discussion by Ritter et al. 2007).

Whilst the overall structure of the rift is well established, it is difficult to determine the active faults of the rift in detail. Therefore, the second author of this paper covered a number of sections within the rift and at the rift margins with EMR line measurements. One of these sections across the eastern rift margin is displayed in Figure 4b. It shows the major rift margin fault as a steeply W dipping structure. In addition, minor faults in the adjacent rift shoulder can also be identified. They dip steeply towards the rift.

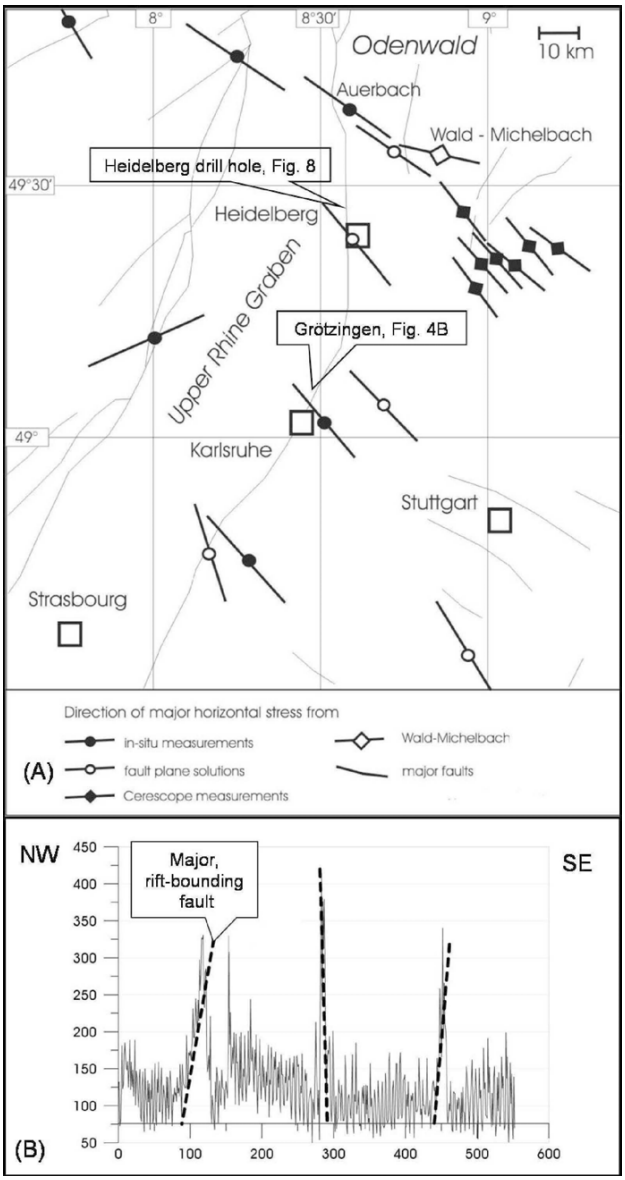

Fig.4. (a) Tectonic map of the north-central part of the Upper Rhine Graben rift with available data on maximum horizontal stress directions (Reinecker et al. 2004; Lichtenberger, 2006b). The locations of the section in (b) and of the Heidelberg research drill hole (see Fig. 8) are indicated. **(b)** EMR section across Rhine rift marginal faults at Grötzingen, NE of Karlsruhe (49°01'37.45"N 08°30'40.45"E to 49°01'36.22"N 08°30'46.96"E). Horizontal length in m, vertical scale in arbitrary energy units. Thick dashed lines show interpretation of anomalies as due to zones of stress concentrations and potentially active faults.

EMR at Intraplate Compressional Structures in the Kachchh Region, NW India

As an example of EMR results in an area of recent convergence and transpression, Figure 5c shows a section across a thrust fault and related anticline from the Kachchh Mainland Fault (KMF) in the Kachchh basin of NW India (Fig. 5b). The Kachchh basin originated as a rift basin with subsidence along normal faults and sedimentary infill. A subsequent inversion stage led to buckling, uplift, block rotation along normal faults (Biswas, 1987), and fault-related folding along the thrusts (Mathew et al. 2006; Karanth and Gadhavi, 2007). The Kachchh basin is also known for its recent recurrent earthquake episodes and has experienced moderate to large earthquakes from historic to modern times (Malik et al., 1999; Karanth et al. 2001; Biswas and Khattri, 2002). Therefore, the Kachchh basin provides a classic example of structural inversion. The inverted faults trend E-W, and associated ridges represent fault-related anticlines (Mathew et al. 2006). The forelimbs and backlimbs of these anticlines show slickensides associated with bedding parallel shear surfaces. In places, graben structures are observed along the hinge zone of anticlines due to tensile fracturing. The section (Fig.5c) is taken from the recent work by Mallik et al. (2008) and shows EMR signals, which are emitted both from low angle surfaces and from more steeply inclined surfaces. Whilst the low angle surfaces can be correlated with bedding-slip surfaces, the steeply dipping surfaces correspond to extensional faults observed at the fold hinge (Mallik et al. 2008; Fig.5c).

VERTICAL SECTION EMR MEASUREMENTS IN TUNNELS AND 3D STRESS DISTRIBUTION

As outlined above, EMR deter-minations in the underground may be performed by taking directional measurements along a vertical circle, normal to the tunnel axis (Fig. 3b, c). Apart from the engineering geological results in terms of tunnel stability, such EMR data also provide information on the regional stress field both with regard to its direction and its magnitude. The first example from the Swiss Jura shows directional results, whilst the second example from Scandinavia also gives stress values.

The Swiss Jura Fold-and-Thrust Belt

The Swiss Jura is part of the marginal fold-and-thrust belt of the Alpine orogen and one of the classic examples of a thin-skinned fold-and-thrust belt (e.g. Mosar, 1999; Becker, 2000; Madritsch et al. 2008). It overlies autochthonous, crystalline basement of Variscan age with a discontinuous cover of late Permian and early Triassic clastic sequences. Mid- to late-Triassic evaporites acted as detachment horizons, mostly “Gipskeuper” in the S and anhydrite of mid-Muschelkalk age in the N. The overlying sequences of

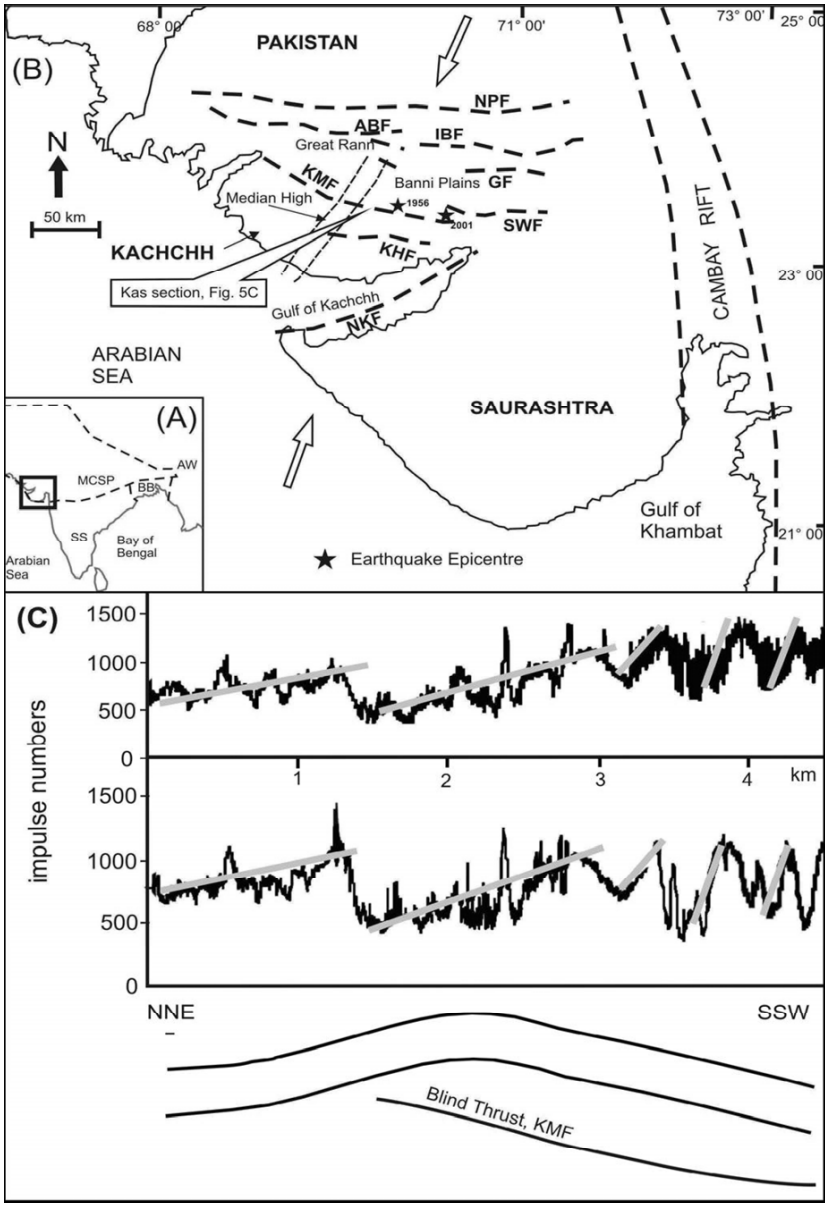

Fig.5. (a) Location of the Kachchh area (box) within the stress provinces of central southern Asia: Mid-Continental Stress Province (MCSP), Southern Shield (SS), Bengal Basin (BB) and Assam Wedge (AW). **(b)** Major fault zones of the Kachchh area (thick, dashed lines) and the direction of the recent maximum horizontal stress (open arrows), redrawn from Mallik et al. (2008). NPF: Nagar Parkar Fault, ABF: Allahbund Fault, IBF: Island Belt Fault, GF: Gedi Fault, KMF: Kachchh Mainland Fault, SWF: South Wagad Fault, KHF: Katrol Hill Fault, NKF: North Kathiawar Fault. The location of an EMR section across the KMF at Kas as shown in (c) is indicated. **(c)** EMR section measurements across the antiform overlying the blind fault tip of the Kachchh Mainland thrust fault (KMF), redrawn from Mallik et al. (2008). The section was measured twice in order to test the reliability and variation of the EMR results. Grey lines show the interpretation of anomalies as due to layer-parallel slip surfaces (shallow dips) at the steep limb of the KMF tip fold and extensional fractures at the hinge and the shallow limb (steep dips). The third section at the bottom gives a schematic view of the structure, inspired by Mathew et al. (2006) and Karanth and Gadhavi (2007).

Jurassic limestones with subordinate shales were thrusted and folded at a late stage of Alpine orogeny in late Neogene times. The Swiss Jura occupies the NW corner of the orogen, at the northern end of the western Alpine arc. Accordingly, the folds and thrusts curve from E-W directions in the E to N-S in the SW (Fig. 6a, b), and reflect tectonic transport from the interior of the orogen in the SE towards the foreland. Folds dominate in the western part and thrusts in the north-east. Strike-slip faults acted as transfer zones between folds and thrusts. From this deformation pattern, the syn-deformational maximum horizontal stress directions can be assumed as normal to the folds and thrusts, i.e. radially away from the centre of the western Alpine arc.

Determinations of the recent stresses show a different pattern, with two distinct directions of maximum horizontal stress, N-S in the centre and the SW of the arc, and NW-SE in the SE, E, and NW of the Jura belt (Becker, 1999; 2000). Subsequent work by the second author of this paper in road and railway tunnels allowed to deter-mine maximum horizontal stresses at numerous further locations and at different structural levels within the Swiss Jura and its autochthonous foreland (Fig. 6). Results from autochthonous basement rocks and their cover show fairly uniform NW-SE directions (N135ºE ± 5º). This direction compares well with the results of earlier stress determinations by other, traditional methods and by earthquake data (e.g. Becker, 1999; 2000; Reinecker et al. 2004, Madritsch et al. 2008). These directions are also typical for the wider region of the European plate north of the Alps (compare with Reinecker et al. 2004, and Lichtenberger, 2006a, b, c). In contrast to these stress directions, results from the allochthonous rocks of the fold-and-thrust belt show maximum horizontal stress directions varying from N-S to NE-SW (c. N05ºE-N50ºE). These recent stress directions in the allochthonous rocks are generally

oriented subparallel with adjacent strike-slip faults (Fig. 6b).

These data imply that the detachment horizon at the base of the Swiss Jura fold-and-thrust belt presently acts as a boundary between two tiers, which have distinctly different stress fields. This result is consistent with observations by Madritsch et al. (2008) of local decoupling between basement and cover in the area adjacent to the west. These authors presume a thick-skinned recent tectonic activity at a regional scale, due to compression and underplating in the Alpine foreland. Alternatively, the stress pattern in the upper tier may be gravity driven and caused by the topographic load of the Alps in the S and SE.

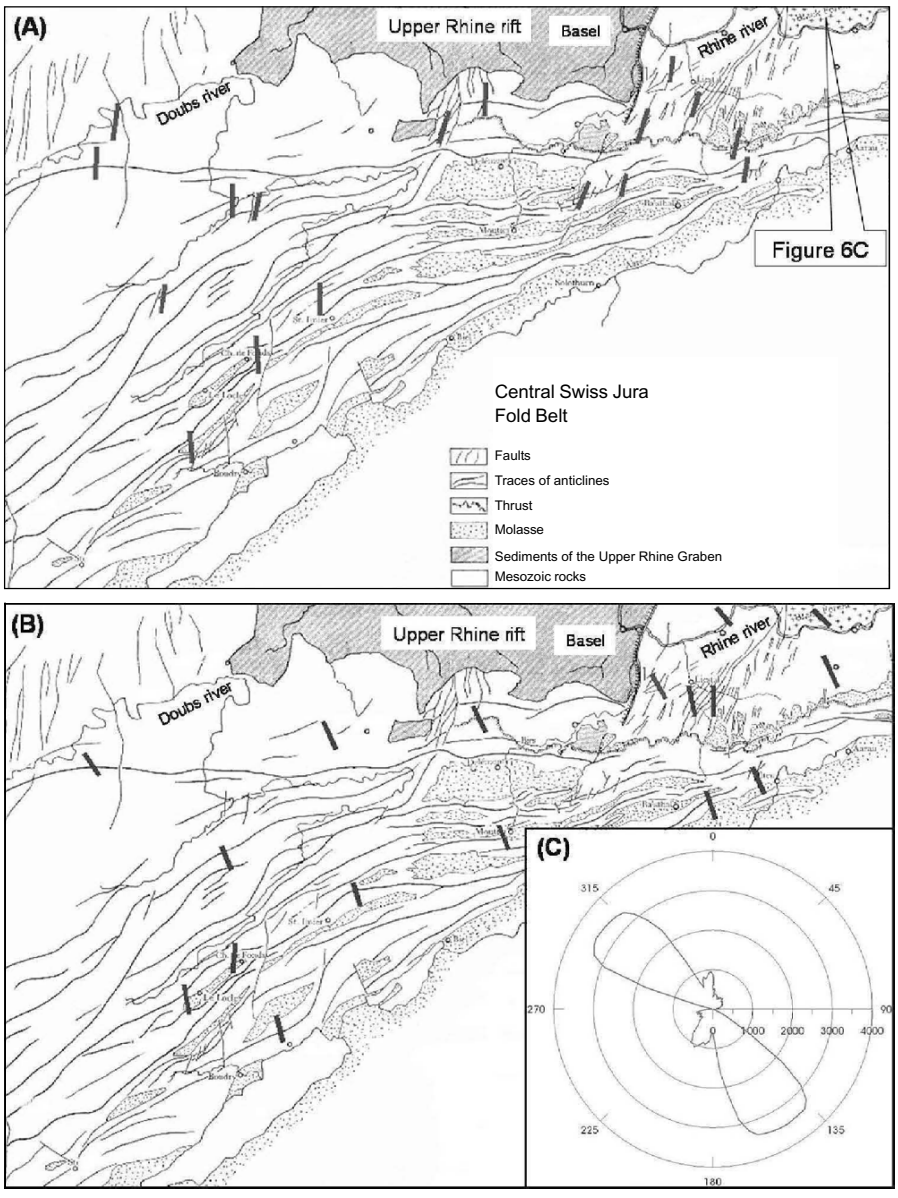

Fig.6. Tectonic maps of the NE and central Swiss Jura fold-and-thrust belt and available data on recent maximum horizontal stress directions (shown as thick black lines) from **(a)** the tier below the basal detachment and **(b)** above the detachment (compiled from Becker, 1999, 2000, and Obermeyer, unpublished data). **(c)** Example of EMR directional data from the tier below the detachment of the Swiss Jura, in the adjacent Black Forest (Rickenbach, 47°37'0.75"N 7°57'1.61"E). The location of the diagram is indicated on (a), scale in arbitrary energy units.

Neotectonics in a Part of West-central Scandinavia

The western margin of Scandinavia is dominated by the Scandinavian Caledonides of Palaeozoic age, which overlie the older continental basement of the Fennoscandian Shield. This area is a classic one for plate tectonics and the Wilson cycle, where the break-up of Rodinia, the formation and subduction of the Iapetus Ocean, the formation of Laurussia, and, finally, the development of the North-Atlantic Ocean are well documented (see Gayer, 1985; 1989; Gee and Sturt, 1985; Lundqvist and Autio, 2000; Eide, 2002; Roberts et al. 2007). The most obvious structural imprint is that of Caledonian convergence, compression, and transpression. However, these structures were reactivated and/or overprinted by late Caledonian extension and by subsequent brittle deformation throughout Mesozoic and Cainozoic times (e.g. Fossen and Rykkelid, 1992; Eide, 2002; Osmundsen et al. 2003). Recent tectonic activity, as it is expressed by post-glacial faults and recent earthquakes, may either be related to the effects of post-glacial rebound following the removal of the load of the late Pleistocene inland ice, or to plate tectonic effects, probably the ridge push of the North-Atlantic mid-ocean ridge (e.g. Eide, 2002; Fredén, 1994).

During a sequence of EMR surface measurements it was also possible to determine EMR in a tunnel, the Steinf-jellet road tunnel in NE Trøndelag, Norway. This tunnel cuts across one of the major Caledonian shear zones, the nappe

boundary between the Upper and the Uppermost Allochthons, which also represents the suture between oceanic (Iapetus) terranes , and a continental, active margin terrane (Laurentia, Roberts et al. 2007). This suture acted as a compressional shear zone during Caledonian convergence and was overprinted by late Caledonian transtensional deformation (Osmundsen et al. 2003). Subsequently, it may have been reactivated during strike-slip movement at the Møre-Trøndelag fault zone in Mesozoic times, and during extension in the North-Atlantic realm during Mesozoic and Cainozoic times (e.g. Eide, 2002). Figure 7a shows the location of the Steinfjellet tunnel in west-central Scandinavia together with the available directions of recent maximum stresses, which are WNW-ESE to NW-SE. The results of EMR cross section measurements in the Steinfjellet tunnel are compiled in Fig.7b. The height of the overburden allows to calculate the vertical stress component. Based on this information, the EMR signals can be related to maximum shear stress values (Lichtenberger 2005; 2006b; see also section measurement methods, above). A significant change in impulse numbers and stress magnitude occurs at c. 900m southeast of the northwestern tunnel entrance, with a sudden increase from less than 2000 to more than 3000 (Fig.7b). At

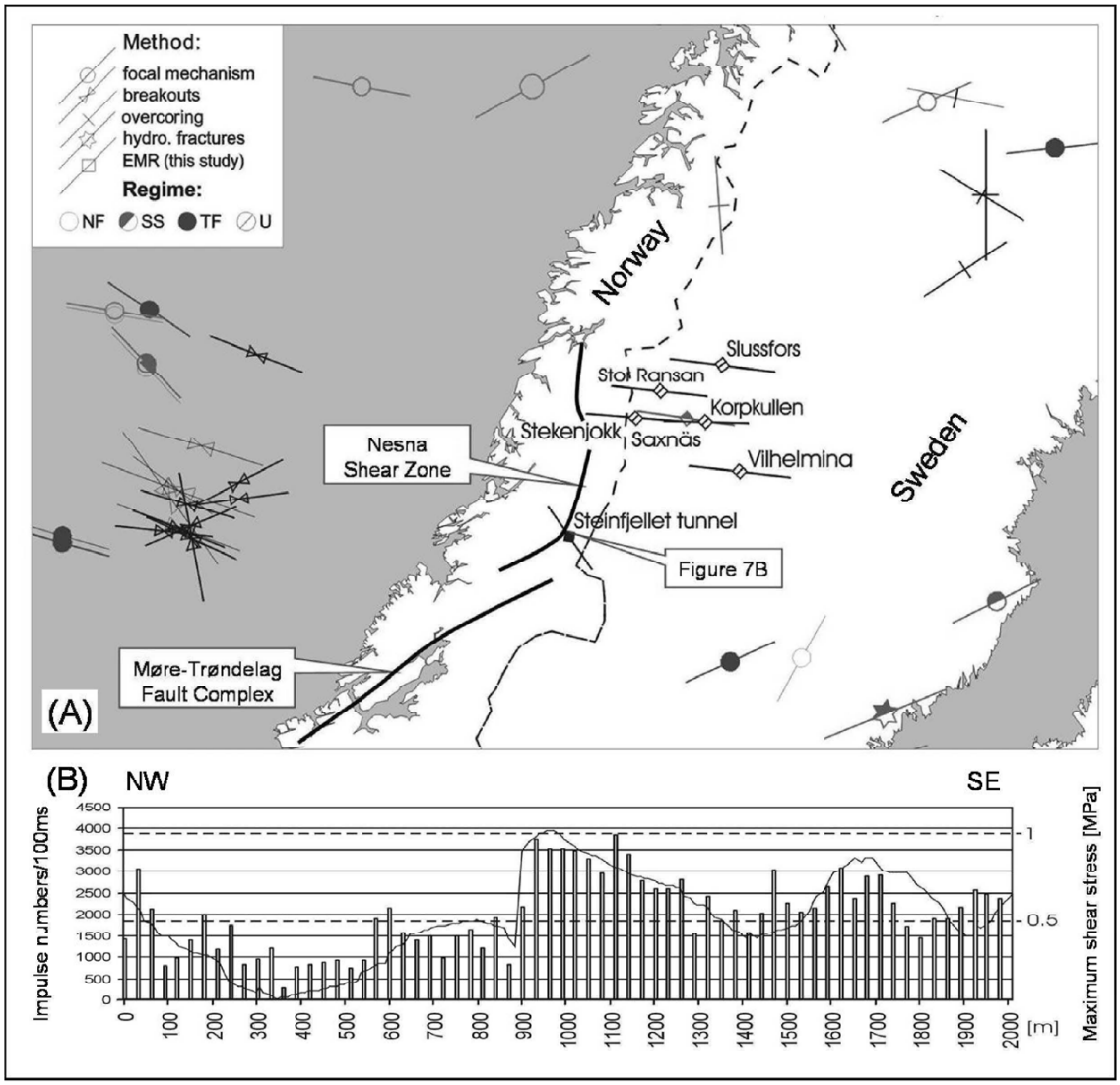

Fig.7. (a) Map of central Scandinavia with available stress data, compiled from Reinecker et al. (2004) and Lichtenberger (2005, unpublished report). Parts of the Nesna Shear Zone and the Møre-Trøndelag Fault Complex, respectively, are taken from Osmundsen et al. (2003). Note location of Steinfjellet tunnel cutting across the Nesna Shear Zone. **(b)** EMR results from the Steinfjellet tunnel, between 64°53'17.40"N 13°12'51.60"E (left) and 64°54'23.40"N 13°15'15.60"E (right), redrawn from Lichtenberger (2005, unpublished report). For location see (a). Note a distinct change in the anomaly pattern at around 900m from the northwestern entrance, where the Nesna Shear Zone is located.

this position the major structural boundary between the Upper and Uppermost Allochthons, which was reactivated as the late Caledonian Nesna Shear Zone, has been mapped at the surface, i.e. above the tunnel (e.g. Osmundsen et al. 2003). Accordingly, the observed change in stress indicates the location of the major, regional shear zone or fault. As is obvious from the stress results, this shear zone is also a boundary of different recent stress domains. Therefore, it can be regarded as still being active and in a state of reactivation.

DISCUSSION

The presented examples show EMR determinations and their results, which can be interpreted in terms of recent stresses and their spatial distribution. These results are useful for solving problems of applied geology, for example, stress concentrations in tunnel walls, which may lead to failures, or the distribution of stresses at slopes, which may indicate active slides or similar phenomena. Applications of EMR during the last decade have demonstrated their use and reliability (see, e.g. Frid 1997, 2001; Liu and He, 2001; Obermeyer et al. 2001; Lauterbach 2002; Bahat et al. 2005; Wang et al. 2005). Figures 5c and 8a show the good reproducibility of EMR measurement results.

However, for future scientific applications it will be necessary to add detailed structural geological studies. At the outcrop scale, the distribution and orientation of fractures, joints, and faults are an important complement (e.g. Lichtenberger 2005). Similarly, microstructural studies will have to show the character and distribution of fractures as related to the rock fabric and individual mineral grains (e.g. Mallik et al. 2008). Ultimately, electron microprobe studies may be carried out towards the aim of documenting the very fractures that emit the measured EMR signals. In that way, it may be possible to provide positive evidence on the origin of EMR from fracturing minerals or rock materials. Such evidence is also needed in order to advance a theoretical physical model for the origin of EMR (see discussions by Bahat et al. 2005; Lichtenberger, 2006c).

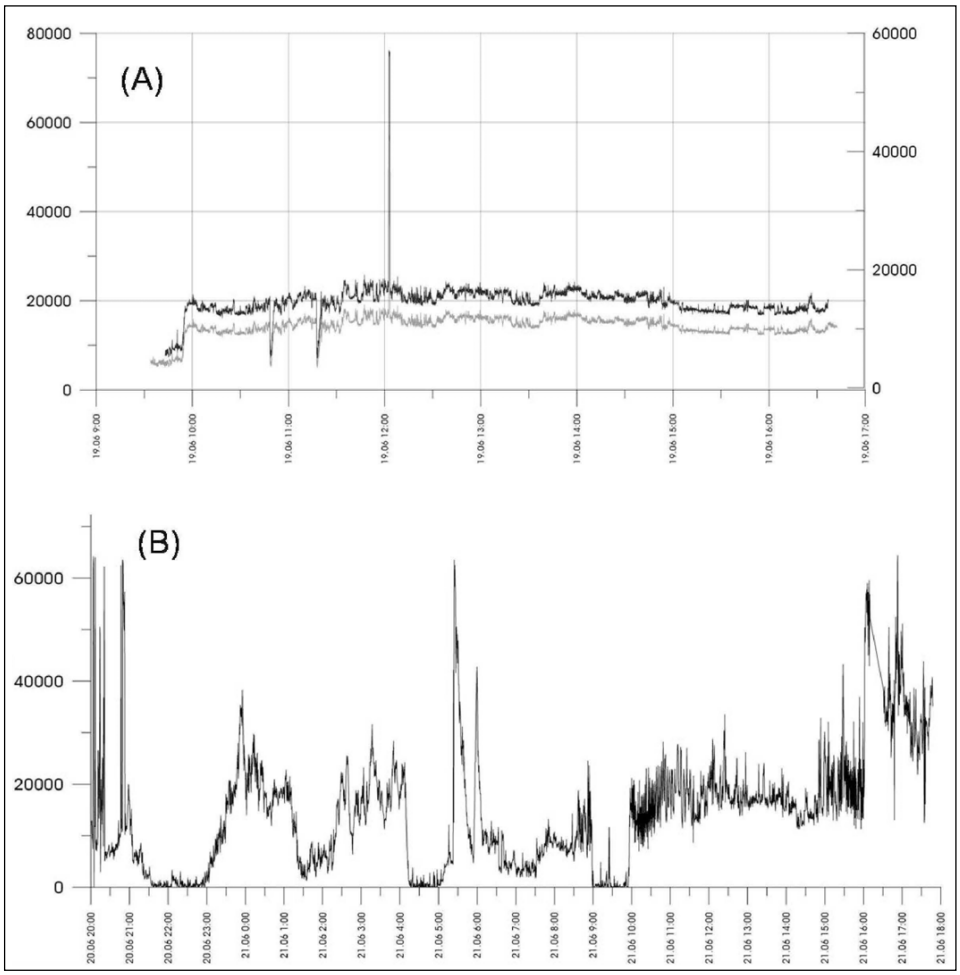

Fig.8. (a) EMR signals at two fixed stations, located at the Heidelberg research drill hole (49°25' 37.64"N 8°39'43.70"E, location on Fig.4a; horizontal scale in hours, vertical scale in arbitrary energy units). The black curve at the top refers to the station at the drill site itself (scale at left), the grey one (bottom, scale at right) to a station 5km farther north. Note good comparability, even for an exceptionally high signal, which is probably anthropogenic. **(b)** EMR signals over 24 hours (June, 20th to 21st, 2008) from the Heidelberg drill site, as in (a). Note strong variation in intensities, which may represent both tectonic, "spheric", and anthropogenic signals.

A different aspect concerns continuous observations of EMR signals and their possible variations with time, for example, dependence on tidal movements or extraterrestrial, astronomic influences. Detailed measurements over time intervals of hours showed variations, which may be relatively small and perhaps related to earth tides (Fig. 8). However, there are also more intense distur-

bances, which may last for seconds (e.g. peak in Fig. 8a), but which may also cover periods of hours (e.g. variations in Fig. 8b, in particular some "lows"; see also Lichtenberger, 2006b, c). These disturbances, sometimes called "spherics", call for continuous observations of EMR signals. Such observations may help to show whether EMR variations are related to variations in lithospheric stress at different time scales (e.g. Bahat et al. 2005; Rabinovitch et al. 2007), and may reflect stress variations during and between earthquake events.

Acknowledgements: Studies in the Upper Rhine Graben rift are part of the EUCOR URGENT research project. The Heidelberg research drill hole was organized by GGA, now Leibniz Institute for Applied Geophysics (Hannover) and LGRB (Freiburg). We thank these institutions, in particular D. Ellwanger and G. Gabriel, and the drilling company Daldrup and Söhne AG for their cooperation. EMR determinations in Scandinavia were carried out during field work for the PNASTINA project on natural building materials. We thank Olof Forslund (SGU, Malå) and Örjan Einarsson (Geopartner AB, Vilhelmina) for their cooperation. Reviews by V. Frid as well as suggestions by D. Ellwanger and the Editor, M.A. Mamtani, provided for numerous improvements and are gratefully acknowledged.

References

Bahat, D., Rabinovitch, A. and Frid, V. (2005) Tensile fracturing in rocks - tectonofractographic and electromagnetic radiation methods. Springer, Heidelberg. 570p.

Becker, A. (1999) In situ stress data from the Jura Mountains – new results and interpretation. Terra Nova, v.11, pp. 9-15.

Becker, A. (2000) The Jura Mountains – an active foreland fold-and-thrust belt? Tectonophysics, v.321, pp.381-406.

Biswas, S.K. (1987) Regional tectonic framework, structure and evolution of the western marginal basins of India. Tectonophysics, v.135, pp.307-327.

Biswas, S.K. and Khattri, K.N. (2002) A geological study of earthquakes in Kutch, Gujarat, India. Jour. Geol. Soc. India, v.60, pp.131-142.

Cardozo, G.L. and Behrmann, J.H. (2006) Kinematic analysis of the Upper Rhine graben boundary fault system. Jour. Struct. Geol., v.28, pp.1028-1039.

Dèzes, P., Schmid, S.M. and Ziegler, P.A. (2004) Evolution of the European Cenozoic Rift System: interaction of the Alpine and Pyrenean orogens with their foreland lithosphere. Tectonophysics, v.389, pp.1-33.

Eide, E.A. (coord.) (2002) BATLAS – Mid Norway plate reconstruction atlas with global and Atlantic perspectives. Geological Survey of Norway, Trondheim, 75p.

Fossen, H. and Rykkelid, E. (1992) Postcollisional extension of the Caledonian orogen in Scandinavia: structural expressions and tectonic significance. Geology, v.20, pp.737-740.

Fredén, C. (Ed.) (1994) Geology. National Atlas of Sweden. Almqvist & Wiksell, Stockholm, 208p.

Frid, V. (1997) Electromagnetic radiation method for rock and gas outburst forecast. Jour. Applied Geophys., v.38, pp.97-104.

Frid, V. (2001) Calculation of electromagnetic radiation criterion for rock burst hazard forecast in coal mines. Pure and Applied Geophys., v.158, pp.931-944.

Gayer, R.A. (Ed.) (1985) The tectonic evolution of the Caledonide-Appalachian orogen. Vieweg, Braunschweig/Wiesbaden, 194p.

Gayer, R.A. (Ed.) (1989) The Caledonide geology of Scandinavia. Graham & Trotman, London, 312p.

Gee, D.G. and Sturt, B.A. (Eds.) (1985) The Caledonide Orogen - Scandinavia and Related Areas. John Wiley & Sons, Chichester, 1266p.

Haimberger, R., Hoppe, A. and Schäfer A. (2005) High-resolution seismic survey on the Rhine River in the northern Upper Rhine Graben. Internat. Jour. Earth Sci., v.94, pp.657-668.

Karanth, R.V., Sohoni, P.S., Mathew, G. and Khadkikar, A.S. (2001) Geological observations on 26th January 2001 Bhuj earthquake. Jour. Geol. Soc. India, v.58, pp.193-201.

Karanth, R.V. and Gadhavi, M.S. (2007) Structural intricacies: emergent thrusts and blind thrusts of Central Kachchh, western India. Current Science, v. 93, pp. 1271-1280.

Lauterbach, M. (2002) Monitoring historic rockfall deposits near Dornbirn, Austria, with the NPEMFE-Method (natural pulsed electromagnetic field of Earth), Excursion Guide. CERG Intensive Course 2002, Amsterdam (RFASE) and Dornbirn (Vorarlberger Naturschau), pp.105-107.

Lichtenberger, M. (2005) Regional stress field as determined from electromagnetic radiation in a tunnel. Jour. Struct. Geol., v.27, pp.2150-2158.

Lichtenberger, M. (2006a) Determination of horizontal principal directions of stress in the Lower Muschelkalk in Northern Baden-Württemberg (Germany) from geogenic electromagnetic radiation. Neues Jahrbuch für Geologie und Paläontologie Abhandlungen, v.238, pp.279-312.

Lichtenberger, M. (2006b) Underground measurements of electromagnetic radiation related to stress induced fractures in the Odenwald mountains (Germany). Pure and Applied Geophys., v.163, pp.1661-1677.

Lichtenberger, M. (2006c) Bestimmen von Spannungen in der Lithosphäre aus geogener elektromagnetischer Strahlung. Gaea heidelbergensis, v.16, ISSN 1612-5452.

Liu, M. and He, X. (2001) Electromagnetic response of outburst prone coal. Internat. Jour. Coal Geol., v.45, pp.155-162.

LUNDQVIST, T. and AUTIO, S. (Eds.) (2000) Description to the Bedrock Map of Central Fennoscandia (Mid-Norden). Geol. Surv. Finland, Spec. Paper, v.28, 176p.

MADRITSCH, H., SCHMID, S.M. and FABBRI, O. (2008) Interactions between thin- and thick-skinned tectonics at the northwestern front of the Jura fold-and-thrust belt (eastern France). Tectonics, v.27, TC5005, doi:10.1029/2008TC002282, 2008.

MALIK, J.N., SOHONI, P.S., KARANTH, R.V. and MERH, S.S. (1999) Modern and historic seismicity of Kachchh peninsula, western India. Jour. Geol. Soc. India, v.54, pp.545-550.

MALLIK, J., MATHEW, G., ANGERER, T. and GREILING, R.O. (2008) Determination of directions of horizontal principal stress and identification of active faults in Kachchh (India) by Electromagnetic Radiation (EMR). Jour. Geodynamics, v.45, pp.234-245.

MATHEW, G., SINGHVI, A.K. and KARANTH, R.V. (2006) Luminescence chronometry and geomorphic evidence of active fold growth along the Kachchh mainland fault (KMF), Kachchh, India, Seismotectonic implications. Tectonophysics, v.422, pp.71-87.

MILSOM, J. (2003) Field Geophysics. John Wiley & Sons, Chichester, 232p.

MOSAR, J. (1999) Present-day and future tectonic underplating in the western Swiss Alps; reconciliation of basement/wrench-faulting and decollement folding of the Jura and Molasse Basin in the Alpine Foreland. Earth Planet. Sci. Lett., v.173, pp.143-155.

OBERMEYER, H., LAUTERBACH, M. and KRAUTER, E. (2001) Monitoring landslides with natural electromagnetic pulsed radiation. *In:* M. Kühne, H.H. Einstein, E. Krauter, H. Klapperich and R. Pöttler (Eds.), International Conference on Landslides 2001, pp.297-304.

OSMUNDSEN, P.T., BRAATHEN, A., NORDGULEN, O., ROBERTS, D., MEYER., G.B. and EIDE, E. (2003) The Devonian Nesna shear zone and adjacent gneiss-cored culminations, north-central Norwegian Caledonides. Jour. Geol. Soc. London, v.160, pp.137-150.

PARASNIS, D.S. (1996) Principles of Applied Geophysics. Chapman & Hall, London, 456p.

PETERS, G. (2007) Active tectonics in the Upper Rhine Graben - Integration of palaeoseismology, geomorphology, and geomechanical modelling. Logos Verlag, Berlin, 270p.

PETERS, G. and VAN BALEN, R.T. (2006) Pleistocene tectonics inferred from fluvial terraces of the northern Upper Rhine Graben, Germany. Tectonophysics, doi:10.1016/j.tecto. 2006.10.008

RABINOVITCH, A., BAHAT, D. and FRID, V. (1996) Emission of electromagnetic radiation by rock fracturing. Zeitschrift für Geologische Wissenschaften, v.24, pp.361-368.

RABINOVITCH, A., BAHAT, D. and FRID, V. (2002) Similarity and dissimilarity of electromagnetic radiation from carbonate rocks under compression, drilling, and blasting. International Journal of Rock Mechanics and Mining, v.39, pp.125-129.

RABINOVITCH, A., FRID, V. and BAHAT, D. (2007) Surface oscillations - a possible source of fracture induced electromagnetic radiation. Tectonophysics, v.431, pp.15-21.

REINECKER, J., HEIDBACH, O., TINGAY, M., CONNOLLY, P. and MÜLLER, B. (2004) The 2004 release of the World Stress Map (available online at www.world-stress-map.org).

REUTHER, C., OBERMEYER, H., REICHERTER, K., REISS, S., KAISER, A., BUCHMANN, T., ADAM, J., LOHRMANN, J. and GRASSO, M. (2002) Neotektonik und aktive Krustenspannungen in Südost-Sizilien und ihre Beziehungen zur regionalen Tektonik im Zentralen Mittelmeer. Mitteilungen aus dem Geologisch-Paläontologischen Institut der Universität Hamburg, v.86, pp.1-24.

REUTHER, C.-D. and MOSER, E. (2007) Orientation and nature of active crustal stresses determined by electromagnetic measurements in the Patagonian segment of the South America Plate. Internat. Jour. Earth Sci., v.97, DOI 10.1007/s00531-007-0273-0.

RITTER, J.R.R., WAGNER, M., BONJER, K.-P. and SCHMIDT, B. (2007) The 2005 Heidelberg and Speyer earthquakes and their relationship to active tectonics in the central Upper Rhine Graben. Internat. Jour. Earth Sci., v.97, DOI 10.1007/s00531-007-0284-x

ROBERTS, D., NORDGULEN, Ø. and MELEZHIK, V. (2007) The Uppermost Allochthon in the Scandinavian Caledonides: From a Laurentian ancestry through Taconian orogeny to Scandian crustal growth on Baltica. *In:* R.D. Hatcher, Jr., M.P. Carlson, J.H. McBride and J.R. Martínez Catalán (Eds.), 4-D Framework of Continental Crust: Geol. Soc. Amer. Mem., v.200, pp.357-377, doi: 10.1130/2007.1200(18).

ROTSTEIN, Y., SCHAMING, M. and ROUSSE, S. (2005) Structure and Tertiary tectonic history of the Mulhouse High, Upper Rhine Graben: Block faulting modified by changes in the Alpine stress regime. Tectonics, v.24, 2004TC001654.

SCHUMACHER, M.E. (2001) Upper Rhine Graben: Role of pre-existing structures during rift evolution. Tectonics, v.21, 2001TC900022.

WANG, E., HE, X., DOU, L., ZHOU, S., NIE, B. and LIU, Z. (2005) Electromagnetic radiation characteristics of coal and rocks during excavation in coal mine and their application. Diqiu Wulixue Bao = Acta Geophysica Sinica, v.48, pp.216-221.

(Received: 1 February 2009; Revised form accepted: 28 June 2009)